

Surface-extended x-ray-absorption fine-structure experiments at atmospheric pressure by means of a photocathode proportional counter with monolayer sensitivity

G. G. Long

National Institute of Standards and Technology, Gaithersburg, Maryland 20899

D. A. Fischer

Exxon P.R.T. at Brookhaven National Laboratory, Bldg. 510E, Upton, New York 11973

J. Kruger

The Johns Hopkins University, Baltimore, Maryland 21218

D. R. Black

National Institute of Standards and Technology, Gaithersburg, Maryland 20899

D. K. Tanaka

The Johns Hopkins University, Baltimore, Maryland 21218

G. A. Danko

*The Johns Hopkins University, Baltimore, Maryland 21218
and National Institute of Standards and Technology, Gaithersburg, Maryland 20899*

(Received 11 July 1988)

Surface-extended x-ray-absorption fine-structure measurements at atmospheric pressure were made by means of a new photocathode proportional counter on the oxide films that form on bulk iron substrates. Both thermally formed and chemically formed films were studied. Near-edge spectra with effective monolayer sensitivity were used to investigate the ionicity of cations in ultrathin films.

I. INTRODUCTION

Soon after the introduction of the extended x-ray-absorption fine-structure (EXAFS) technique as a structural tool, it was extended to include surface-sensitive measurements. The earliest surface-EXAFS measurements involved fluorescence detection of photons from ultrathin films on copper.¹ The difficulty with these measurements is that if the absorption edge to be measured is of an element present in both the bulk and in the surface layers, then the signal that is obtained may be dominated by the bulk structure. A solution to this bulk sensitivity problem was first proposed by Shevchik and Fischer,² who introduced the photocathode ionization chamber for surface EXAFS.

The sample, in the photocathode ionization chamber experiment, is a surface film on a flat plate inside the detector volume. The detector is supplied with flowing helium, which nominally does not absorb the incident hard x rays. The sample does absorb the x rays and emits electrons, which are collected over a large solid angle and may be amplified through field-intensified ionization in the helium gas. A tungsten wire anode collects these electrons and the current passing through the detector is measured. This experiment is similar to a partial electron-yield³ experiment, which ordinarily must be performed in an ultrahigh vacuum. In the electron-yield experiment Auger electrons, photoelectrons, secondary

electrons, and inelastic electrons are counted as a function of the energy of the incident x radiation.

The photocathode ionization chamber² has found application in studies of the oxidation processes of copper,⁴ the structure of solution-formed passive films on iron,⁵ and the structure of surface layers on GaAs.⁶ Measurements with this detector have been shown to be qualitatively more sensitive to surface layers than fluorescence measurements,⁷ to be experimentally comparable to x-ray absorption,⁸ and to have depth selectivity when operated in an electron energy resolving mode.⁹ In the demonstration studies,⁷⁻⁹ the measurements were conducted with the photon beam incident at either 90° or 45° to the sample surface. Although normal-incidence, or 45°, geometry may be convenient, much improved surface sensitivity is achieved with grazing-incidence geometry, as will be demonstrated below. Grazing-incidence geometry has been exploited in a very limited number of studies,³⁻⁵ although earlier work¹⁰ indicated its importance.

While the photocathode EXAFS detector is becoming recognized for its usefulness, a characterization of the phenomena taking place has thus far been neglected. An improved understanding of photocathode detection and a set of rules regarding detector properties would contribute to a more efficient use of these devices and to a wider application to new types of measurements.

In this study, the photocathode detector was first care-

fully characterized to explore its operation both in the current mode as an ionization chamber and in the pulse mode as a proportional counter. The device was then applied to the investigation of the structure of ultrathin films that form on the surface of bulk iron.

EXPERIMENT

Two factors contribute to the surface sensitivity of the photocathode detector: the mean free paths of the electrons which emerge from the surfaces of the samples and the kinetic energies of these electrons in the detector gas. The average depth from which Auger electrons and photoelectrons emerge is 1–3 orders of magnitude smaller than the attenuation length of the x rays. The surface sensitivity of this experiment is expected to improve as the depth of the photoabsorption is made small. This fact suggests grazing-incidence geometry. Secondary electrons and inelastically scattered electrons created several mean free paths below the surface can also emerge, but the detection scheme is weighted against their contribution to the current or pulse signal because of their relatively lower kinetic energies as they are ejected into the detector gas.

Figure 1 shows a cross section of the photocathode ionization chamber or proportional counter experiment. There are two entrance windows, each covered with $6\ \mu\text{m}$ aluminized Mylar, so that measurements can be made in either the normal-incidence geometry or the grazing-incidence geometry. The entire detector may be rotated about the axis shown in Fig. 1. A $25\text{-}\mu\text{m}$ -diam (gold-

plated) tungsten wire serves as the anode, and a removable sample plate serves as the photocathode. The photocathode, which is the sample under investigation, lies within the detector volume, thereby allowing a 2π -sr collection solid angle for electron emission from the surface. The sample can be electrically isolated from the detector to enable the measurement of ion current. To ensure good energy resolution, the ideal cylindrically symmetrical proportional-counter geometry is maintained insofar as possible. The introduction of a flat sample into the curved counter wall introduces some asymmetries into the electric field about the anode wire. This field distortion and that from the grounded end caps were minimized by making the detector diameter large relative to the sample width and small relative to the sample length. The proportional-counter energy resolution was measured using *P*-10 (argon–10%–methane) flow gas and 5.9-keV x rays from an ^{55}Fe radioactive source. The FWHM ($\Delta E/E$) was measured to be 0.23, i.e., close to the literature value of 0.17,¹¹ indicating that, while not ideal, the proportional-counter resolution is good.

For surface-EXAFS measurements, the argon-methane flow gas is replaced with a helium-methane flow-gas mixture that is 99.9% transparent to 7-keV photons in 2 cm of gas. In this situation, photoemission from the counter cathode wall is preferentially enhanced in the counter gas. X rays passing through the gas and impinging on the sample (that is, the counter cathode) will yield an electron spectrum consisting of Auger electrons, photoelectrons, secondary electrons, and inelastic electrons. The emitted electrons will lose their kinetic energy by im-

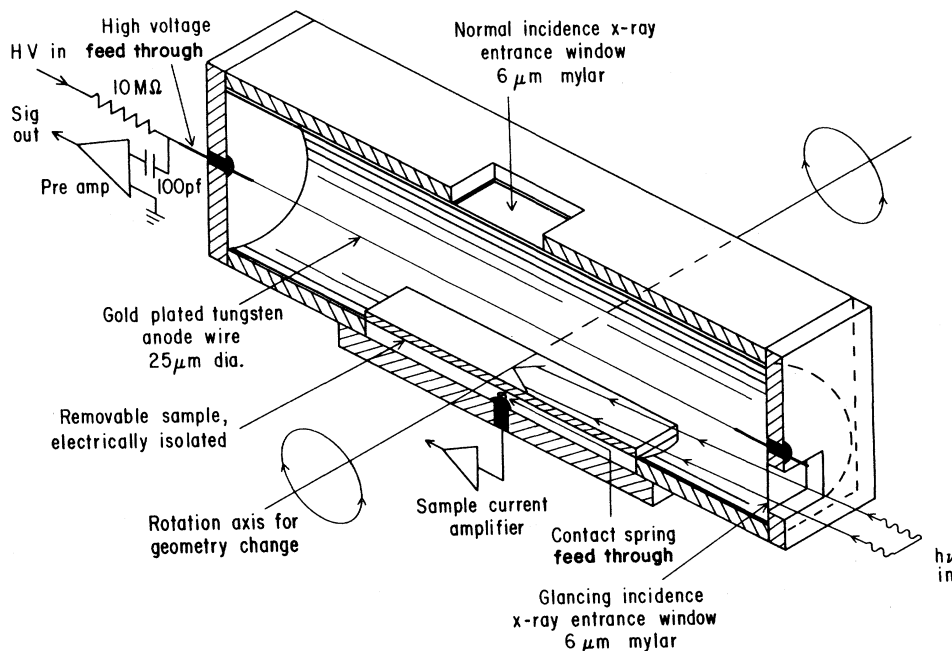


FIG. 1. Cross-sectional view of the photocathode detector. The instrument can be operated in either the normal-incidence geometry or in the glancing-incidence geometry, and either as a photocathode ion chamber or as a photocathode proportional counter.

compact ionization in the helium gas and create a number of electron-ion pairs (40 eV/pair) (Ref. 12) proportional to the original kinetic energy of the ejected electron. If the anode wire voltage is maintained in the proportional region, field-intensified gas multiplication will occur, resulting in charge pulses on the anode again proportional to the original ejected electron kinetic energy. After this amplification, the resulting pulse-height distribution resembles a kinetic energy x-ray photoelectron spectrum (XPS) from the sample convolved with the proportional-counter resolution function.

To understand the efficiency and surface sensitivity of these experiments, and to evaluate the effects of sample geometry, measurements were made by means of the detector shown in Fig. 1 at the N.I.S.T. beamline X-23A3 at the National Synchrotron Light Source, Brookhaven National Laboratory. Data for the detector characterization studies were collected on a thin (20-nm) thermally formed oxide layer on the surface of a bulk (1 mm thick) iron plate.

Pulse-height spectra from the iron-oxide sample are shown in Figs. 2 and 3 for the normal-incidence and grazing-incidence geometries, respectively, and for incident photons of energies below and above the iron *K* edge at 7.112 keV. The count-rate limitations for this detector are similar to those for ordinary proportional counters. All of the present experiments were conducted in the linear range where no dead-time corrections are required.¹³ For the normal-incidence geometry (Fig. 2), there is a prominent photopeak due to the small but non-negligible amount of absorption of the x rays in the helium-methane gas. This peak shifts with increasing photon energy, but its height is constant across the iron *K* edge for equal spectrum accumulation times. Therefore, the photopeak can serve as an energy calibration of the pulse-height spectra. The lower kinetic energy peak in Fig. 2 and its tail correspond to a kinetic energy XPS spectrum of the iron oxide layer for a photon energy of

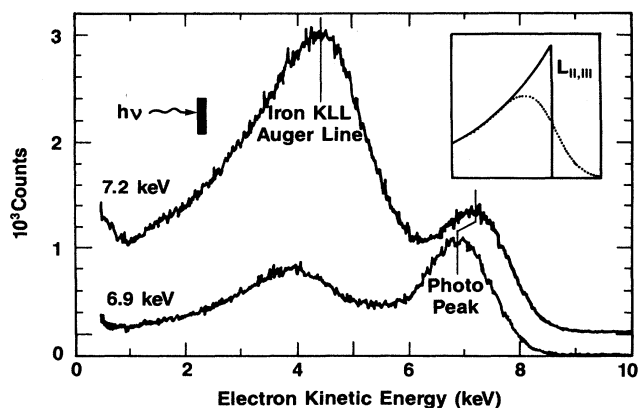


FIG. 2. Electron kinetic energy spectra (i.e., pulse-height spectra) from a thermally formed 20-nm iron oxide film on bulk iron, measured in the normal-incidence geometry. The upper (lower) curve was measured using an incident photon energy above (below) the iron *K* edge. The inset shows an *L*-shell XPS line (solid), and its appearance (dashed) after convolution with the instrument resolution function.

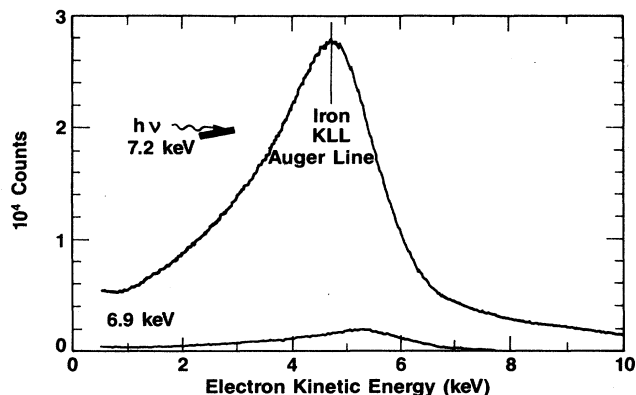


FIG. 3. Electron kinetic energy spectra from a thermally formed 20-nm iron-oxide film on bulk iron, measured in the glancing-incidence geometry.

6.9 keV. Thus *L*, *M*, and *N* shell photoelectrons are produced with decreasing probability in addition to lower-energy Auger electrons (*LMN*, *MNN*, etc.). Since the proportional-counter energy resolution is of the order of 23%, the spectrum is dominated by the most probable electron: in this case, *L*-shell photoelectrons of kinetic energy 6.2 keV ($E_k = 6.9 \text{ keV} - 700 \text{ eV}$). In practice, the peak is observed at lower kinetic energy because its position is determined by the convolution of the *L*-shell XPS line and the proportional-counter resolution function. (See inset to Fig. 2.)

Also present in the pulse-height spectrum is a low-energy tail to the peak resulting from secondary and inelastically scattered electrons copiously produced at high kinetic energies and also observed in early XPS data taken at high x-ray energies.¹⁴ Above the iron *K* edge, the upper curve in Fig. 2, *KLL* Auger electrons (kinetic energy equal to 5.7 keV in this case) have the highest probability of production, as indicated by the fourfold increase in signal upon crossing the iron *K* edge.

Similar measurements were performed in the grazing-incidence geometry. The pulse-height data are shown in Fig. 3 for incidence x-ray energies of 6.9 and 7.2 keV. Compared to the normal-incidence data, both the electron kinetic energy peak of the spectrum taken above the iron *K* edge and that of the spectrum taken below the iron *K* edge are shifted to higher kinetic energies. This is because there is decreased probability that the lowest-energy multiply scattered electrons are produced since the x-ray excitation is limited by the geometry to the near-surface region, i.e., only the first 100–200 nm of the sample plate are illuminated by x rays. This upward shift in energy is larger for the spectrum taken below the *K* edge than that for the spectrum taken above the *K* edge. Also, above the iron *K* edge, there is an order-of-magnitude increase in the Auger *KLL* yield for the grazing-incidence geometry compared to normal incidence, along with the virtual disappearance of the photopeak. The negligible photopeak is the result of shorter paths for the incident photons in the detector gas. The increased electron yield is the result of reducing the

depth of photoabsorption to the near surface region for glancing angles of 1° – 3° . From the pulse-height data, one can conclude that glancing-incidence geometry has superior sensitivity over normal-incidence geometry by more than an order of magnitude in signal strength. In addition, one can enhance the surface selectivity in proportional-counter operation by setting a single-channel analyzer window to accept the higher-energy region of the peak in Fig. 3, i.e., setting a bandpass about the *KLL* Auger line. This is analogous to the Auger yield detection technique for surface-EXAFS measurements, which is usually performed in a vacuum, as introduced by Citrin *et al.*¹⁵

The photocathode proportional counter can also be operated at reduced voltage in the ionization chamber mode. Figure 4 shows the current as a function of applied anode voltage. An anode voltage of 100 V is adequate to avoid either recombination or gas multiplication. A reverse bias is also possible, as shown in Fig. 4, resulting in a similar current being measured. The nature of the signal contribution to either current can be understood in terms of the electron-ion pair products of the energetic electrons entering the detector gas from the sample. For the normal-incidence experiment, energetic electrons (with kinetic energy greater than 45 eV) ejected from the photocathode will create a number of electron-ion pairs (40 eV/pair) proportional to their initial kinetic energy as shown in the solid curve of Fig. 5. The resulting electron or ion current is the integral of the solid curve of Fig. 5. This current, which is measured from the isolated photocathode, is weighted linearly in electron kinetic energy. The results of this analysis emphasize the importance of performing current mode experiments in the grazing-incidence geometry. Otherwise the energetic photopeak of Fig. 5 will be everpresent as an enhanced background.

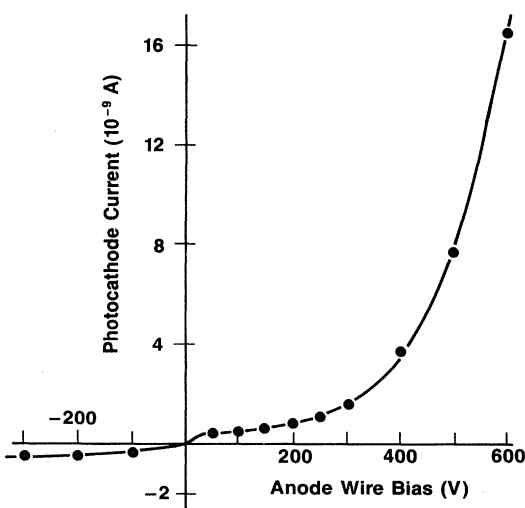


FIG. 4. Photocathode current as a function of the anode wire bias voltage. The data were taken with the 20-nm iron-oxide film sample in place and using photons with energy above the iron *K* edge.

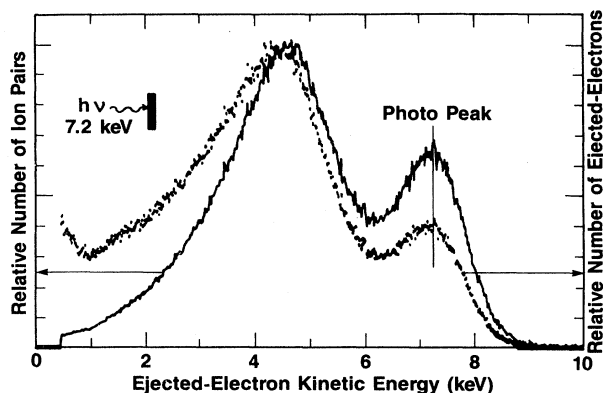


FIG. 5. The dotted curve shows the number of ejected electrons as a function of electron kinetic energy, reproduced from Fig. 2, for the normal-incidence geometry. The solid curve shows the number of ion pairs as a function of electron kinetic energy, which represents the actual signal that is measured in the current mode experiment.

Another important issue in the operation of the photocathode detector in the ionization chamber mode is the observation⁸ of ambiguities in the amplitudes of the fine structure. At the source of this problem is the effective thickness of the surface layers measured and self-absorption in the sample. Three measurements of the 60-eV region about the copper *K* edge are shown in Fig. 6. The dashed curve was taken from a transmission EXAFS experiment on a 4- μ m-thick copper foil. The solid curve is a fluorescence measurement of the same foil. All evidence of EXAFS oscillations are absent. At the *K* edge, one can still see the *K*₁ to *K*₂ transition at the correct position but at the wrong amplitude as the sample goes from optically thin to optically dense. The dot-

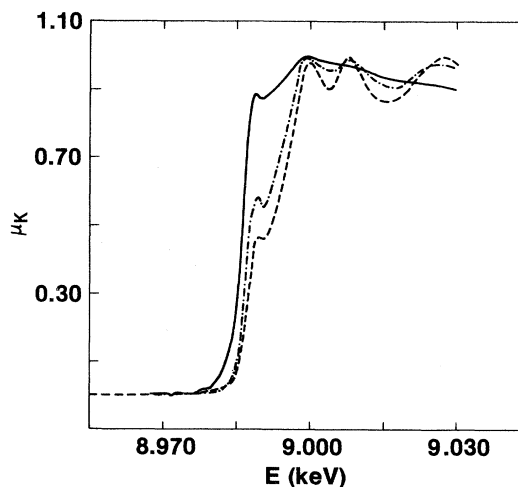


FIG. 6. Near-edge copper *K*-absorption spectra measured from a thin copper foil in transmission (dashed curve), the same thin foil in fluorescence (solid curve), a bulk copper plate in the photocathode detector (dot dashed curve).

dashed curve was taken using the photocathode ionization chamber in the grazing-incidence geometry. While the EXAFS oscillations are clearly visible and one can easily prove that their phase is correct, their amplitude is reduced and the amplitude of the edge feature is incorrect. This result suggests that this photocathode detector measurement, while not optically dense, is also not adequately optically thin. This is despite the advantages in sensitivity of the grazing-incidence geometry mentioned above. Fortunately the problem can be removed entirely, as we demonstrate below, by going over to the photocathode proportional-counter mode, thereby accepting signal only from optically thin layers.

SURFACE-EXAFS AND NEXAFS MEASUREMENTS

The nature and the structure of the passive film that is responsible for the capability of a metal to resist environmental attack are key to developing an understanding of passivity. There have been numerous attempts to determine the nature and the structure of the passive films that grow on iron,¹⁶ from which it is often concluded that the main protective film is cubic Fe_3O_4 at the metal-to-oxide interface and $\gamma\text{-Fe}_2\text{O}_3$ and hydrated oxides at the film-to-air interface. These passive films can be formed chemically by employing a passivating solution,⁵ or by anodic polarization. An important issue has been the role of water or hydrogen and the role of alloying elements such as chromium on the structure of the passive film on iron.

Two surface films on iron were evaluated in this study: the first was a thermally grown oxide on bulk iron, which could be grown to a predetermined thickness, and the second was a chemically grown passive film on bulk iron, which is well known to be ultrathin. The former surface oxide was used as a model compound in the photocathode proportional-counter experiment because its structure is generally understood to consist of Fe_3O_4 and $\gamma\text{-Fe}_2\text{O}_3$, which has a defect structure of Fe_3O_4 . The chemically formed passive film was grown in a potassium-chromate solution because it has been demonstrated⁵ that at least 12% of the cations in this film are chromium. Thus this film can serve as a model for the structure of the passive films that exist on some iron-chromium alloys. The role of chromium is an important issue in the understanding of the improved passive films that are formed on steels. In particular, our aim is to study the structure around the chromium ions in order to better understand their role in the passivation of the surfaces of steel.

Before the films were grown, the bulk iron plates were carefully polished with wet SiC paper, then diamond paste, and finally 0.05- μm alumina. The thermally formed samples were prepared by growing the oxide films at 600 °C for 15 min in a moist oxygen oven. The chemically formed films were grown in 0.005M aqueous potassium-chromate solutions for 72 h, then washed with distilled water, and finally dried with anhydrous ethanol and hot air.

The final film thicknesses were measured by means of a commercial ellipsometer. In this technique, elliptically polarized light is reflected from the surface of interest.

The two orthogonal, s and p , components of the light suffer different changes in phase and amplitude upon reflection. Two pseudo-optical constants are measured: Δ , which is the difference in the phase of the p and s components of the polarized light, and ψ , the tangent of which is the ratio of the amplitudes of the p and s components of the polarized light. These constants are measured for both the bare surface and for the films, and results permit a determination of the thickness of the films. It has been shown that fractions of a monolayer can be measured by means of this technique. The problem associated with precise measurements of surface-layer thicknesses is associated with the accuracy to which the optical constants, n and k , are known. It has been shown¹⁷ that an error of 11% in n and 67% in k produces a maximum error of 0.3 nm (or 7.5%) in a 4-nm film. For thicknesses less than 4 nm, the thickness error bars collapse onto the true value for thickness, even for larger percent errors in n and k . The films used in this study were measured with 546.1-nm light at a 68° angle of incidence and a quarter-wave compensator angle of 45°. The thickness of the thermally grown film was 20 ± 3 nm and the thickness of the chemically grown passive film was 3 ± 2 nm thick.

EXAFS spectra were accumulated in the pulse mode on the same 20-nm oxide film on iron that was used for the pulse-height measurements described above. The bandpass was set to accept the upper $\frac{2}{3}$ of the pulse-height spectrum. This bandpass effectively discriminates against signal coming from iron in the bulk of the photocathode plate. (For reference, transmission absorption spectra measured in the vicinity of the iron K edge are shown in Fig. 7. The solid curve is the background-subtracted K -absorption spectrum for bulk iron; the dashed curve is the same for $\gamma\text{-Fe}_2\text{O}_3$; the dot-dashed is the same for Fe_3O_4 ; and the dot-dot-dashed is the same for $\gamma\text{-FeOOH}$.) The measured absorption spectrum is shown in Fig. 8, where a transmission spectrum of $\gamma\text{-Fe}_2\text{O}_3$ is also shown for comparison. For both spectra, the background due to contributions by other electrons

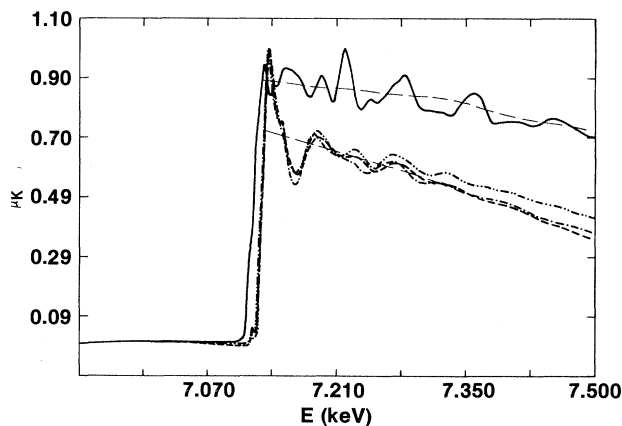


FIG. 7. Background-subtracted iron K -absorption edge spectra for bulk iron (solid curve), for $\gamma\text{-Fe}_2\text{O}_3$ (dashed curve), for Fe_3O_4 (dot-dashed curve), and for $\gamma\text{-FeOOH}$ (dot-dot-dashed curve).

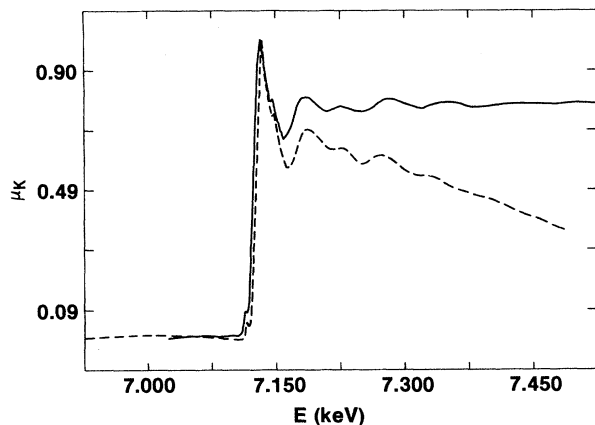


FIG. 8. Background-subtracted iron K edge spectra taken on the 20-nm thermally formed film (solid line) in the photocathode proportional counter and on the model compound $\gamma\text{-Fe}_2\text{O}_3$ (dashed line) in a transmission measurement.

has been subtracted. For the transmission measurement on the model compound, the spectrum above the absorption edge has negative exponential curvature. The photocathode proportional-counter data, by comparison, fall on a flat baseline curve reminiscent of fluorescence data. The Fourier analysis of the EXAFS signal, $\chi(k)$, for these spectra yielded results demonstrating that the surface oxide film and the model compound have very similar structures. Using the $\gamma\text{-Fe}_2\text{O}_3$ results as a model, $r_1(\text{Fe-O})=0.201$ nm and $r_2(\text{Fe-Fe})=0.331$ nm, the measurement of the 20-nm film on bulk Fe yielded $r_2=0.202\pm 0.003$ nm. The $r_2=0.332\pm 0.003$ nm. The coordination numbers for the model were $n_1=5.33$ oxygen atoms and $n_2=10.7$ iron atoms. For the 20-nm film the results were $n_1=5.4\pm 1.1$ oxygen atoms and $n_2=10.9\pm 2.2$ iron atoms. These data indicate that the model and the film spectra have the same phases and amplitudes to within statistical error. It is, furthermore, evident from the raw data that there is no hint of contamination of the surface signal with the bulk iron signal. Evidence of contamination by bulk iron would be easily seen because there is a prominent feature in the iron spectrum at ~ 7.211 keV near the third small oxide oscillation. (See Fig. 7.)

The surface sensitivity of the grazing-incidence geometry was further exploited for current mode measurements on the ultrathin (3-nm) passive film formed on bulk iron in a chromate-passivating solution. As mentioned above, it had been shown earlier⁵ that chromium is present, and that more than 12% of the cations in this film are chromium. Model compounds measured in transmission were chromium metal, finely powdered Cr_2O_3 , and freshly prepared finely powdered CrO_3 . Near-edge chromium K -absorption spectra of these compounds are shown in Fig. 9. The Cr VI spectrum has a distinctive appearance because of the white line¹⁸ that is present in the pre-edge region. This feature has been observed¹⁹ in the absorption spectra of Ti IV, V V, Cr VI, and Mn VII, and is due to a transition from the $1s$ to T_2 empty

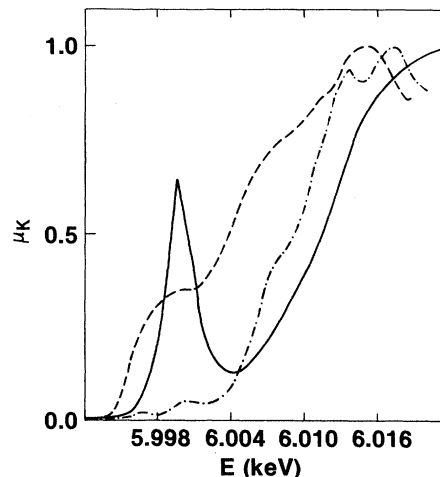


FIG. 9. Model compound spectra for a chromium K edge experiment on chromium oxides. The dashed line is the spectrum for bulk chromium; the dot-dashed line is the spectrum for powdered Cr_2O_3 ; and the solid line is the spectrum of a freshly prepared powder of CrO_3 .

valence orbitals. The chromium spectrum measured by means of the surface-EXAFS photocathode detector is shown in Fig. 10 together with the Cr III and Cr VI model compound spectra. There is a small enhancement of signal in the neighborhood of the Cr VI pre-peak, but the absorption edge position is much closer to Cr III than to Cr VI. This indicates that, although most of the chromium in the film was Cr III, there was also a slight amount of Cr VI in the film. This is an unexpected result because it is difficult to explain how the thin film supports the high oxidation state. Furthermore, the Cr VI appears to be in the film because any Cr VI residue from the passivating solution would have been removed during the rinsing of the film. Additional measurements will be required to

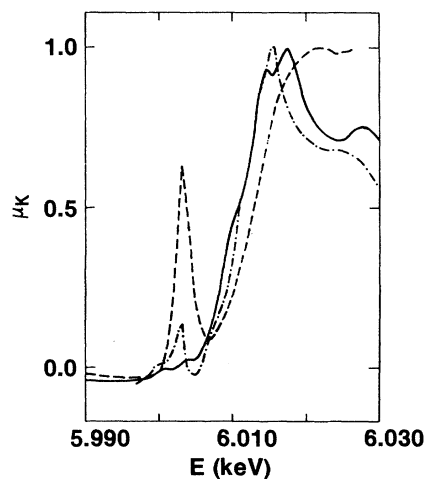


FIG. 10. Near-edge spectrum measured at the chromium K edge for the chromate-formed film (dot-dashed line) on iron. For comparison, the solid line is the Cr_2O_3 spectrum and the dashed line is the spectrum of CrO_3 , each measured in transmission.

evaluate these results. Nevertheless, the quality of the data, taken in a single 30-min scan on a sample with only an approximate monolayer chromium coverage, attests to the sensitivity of the photocathode detector experiment.

CONCLUSIONS

The current work has enabled an improved understanding of the principles of operation of the surface-EXAFS detector, both as a photocathode proportional counter and as a photocathode ionization chamber. For experiments involving elements present in both the bulk and in the surface layers, the proportional-counter operation allows electron kinetic energy selectivity, which in principle can be extended to depth-selective EXAFS mea-

surements through the surface layers. As a photocathode ionization chamber, application in the grazing-incidence geometry offers the best solid-angle detection capabilities and possibly the most efficient monolayer sensitive measurement available.

Future applications of the photocathode proportional counter will almost certainly include the investigation of the layer-by-layer structures of importance in electrochemistry and corrosion, and the investigation of the surface layers of catalysts.

ACKNOWLEDGMENTS

This work was supported in part by the U.S. National Science Foundation through Grant No. DMR-84-190882.

-
- ¹J. A. del Cueto and N. J. Shevchik, *J. Phys. C* **11**, L833 (1978).
²N. J. Shevchik and D. A. Fischer, *Rev. Sci. Instrum.* **50**, 577 (1979).
³J. Stöhr, D. Denley, and P. Perfetti, *Phys. Rev. B* **18**, 4132 (1978); *J. Stöhr, J. Vac. Sci. Technol.* **16**, 37 (1979).
⁴D. A. Fischer, G. G. Cohen, and N. J. Shevchik, *J. Phys. F.* **10**, L142 (1980).
⁵G. G. Long, J. Kruger, D. R. Black, and M. Kuriyama, *J. Electroanal. Chem.* **150**, 603 (1983).
⁶C. E. Bouldin, R. A. Forman, and M. I. Bell, *Phys. Rev. B* **35**, 1429 (1987).
⁷M. E. Kordesch and R. W. Hoffman, *Phys. Rev. B* **29**, 491 (1984).
⁸T. Guo and M. L. den Boer, *Phys. Rev. B* **31**, 6233 (1985).
⁹M. J. Bedzyk and G. Materlik, *Phys. Rev. B* **32**, 4228 (1985).
¹⁰G. Martens, P. Rabe, N. Schwentner, and A. Werner, *J. Phys. C* **11**, 3125 (1978).
¹¹M. W. Charles and B. A. Cooke, *Nucl. Instrum. Methods* **61**, 31 (1968).
¹²W. P. Jesse and J. Sadaukis, *Phys. Rev.* **102**, 389 (1956); **107**, 766 (1957).
¹³J. Fischer, V. Radeka, and G. C. Smith, *Nucl. Instrum. Methods Phys. Res. A* **246**, 511 (1986).
¹⁴K. Seigbahn *et al.*, *Nova Acta Regiae Soc. Sci. Ups.* **20**, 1 (1967).
¹⁵P. H. Citrin, P. Eisenberger, and R. C. Hewitt, *Phys. Rev. Lett.* **41**, 309 (1978).
¹⁶*Passivity of Metals*, edited by R. P. Frankenthal and J. Kruger (The Electrochemical Society, Princeton, 1978).
¹⁷J. Kruger, in *Advances in Electrochemistry and Electrochemical Engineering*, edited by R. H. Muller (Wiley, New York, 1973), Vol. 9, p. 227.
¹⁸M. Brown, R. E. Peierls, and E. A. Stern, *Phys. Rev. B* **15**, 738 (1977).
¹⁹A. Bianconi, E. Frischi, G. Calas, and J. Petiau, *Phys. Rev. B* **32**, 4292 (1985).